Three-dimensional dynamics of detonation cells in linearly diverging channels: experimental analysis of the cross-sectional shape and a detonation-shock dynamics interpretation

Vianney Monnier, Vincent Rodriguez, Ratiba Zitoun, Pierre Vidal

Three-dimensional dynamics of detonation cells in linearly diverging channels: experimental analysis of the cross-sectional shape and a Detonation-Shock Dynamics interpretation

Vianney Monnier, Vincent Rodriguez*, Pierre Vidal, Ratiba Zitoun

Institut Pprime, UPR 3346 CNRS, ISAE-ENSMA, Téléport 2, 1 Avenue Clément-Ader, 86960, Futuroscope-Chasseneuil, France

*Corresponding author: vincent.rodriguez@ensma.fr

June 12, 2024 .

Abstract

We study the transient dynamics of three-dimensional detonation cells when the detonation front is subjected to weak expansion due to the diffraction from a straight channel to an diverging channel. We focus on the effect of the cross-sectional shape, namely square or round, using diverging channels with the same initial cross-sectional area of 16 cm ^{2} as the straight channels and the same expansion rate. The reactive mixture is $2\,H_2 + O_2 + 2\,Ar$ at the initial pressure of 20 kPa and temperature of 294 K, and we use the sooted-foil technique to record the cellular dynamics. The mean cell widths first increase from different initial values, which depend on the cross-sectional shape and then decrease to stabilize at the same value independent of the shape but larger than the initial values. We use a relation of detonation dynamics between the velocity, total curvature and acceleration of the average detonation front to interpret successfully, albeit qualitatively, all the experimental trends. This sensitivity thus makes these experimental data a reliable basis for high-resolution numerical simulations capable of handling three-dimensionality and detailed chemical kinetics mechanisms. Defining a significative mean width of detonation cells requires constant cross-section tubes of size and length sufficiently large. Inductively, representing three-dimensional cells requires more statistical descriptors than a single mean width.

1 Introduction

The reaction zone of detonation in gases has a cellular structure, which is now considered to be an intrinsically 3D phenomenon. For example, we have recently shown that the cross-sectional shape of a straight channel can significantly modify the cellular patterns on detonation fronts when there are not enough cells per unit area on the front of a self-sustained detonation [1]. In the present analysis, we address the case of diverging channels with a round (R) or square (Q) cross-section, focusing on the transient effects on the cell patterns when the detonation front enters the diverging channel from a straight channel. The configuration combines several problems in reactive compressible fluids, from the local scale of the reaction zone to the global scale of the overall curvature and acceleration of the detonation front.

Analysis of the cellular structure still poses experimental, numerical and theoretical problems. Classically, experimental analyses rest on recordings on soot-coated foils placed against the tube

walls (parietal foils) or perpendicular to the tube axis (frontal foils). On parietal foils, the moving intersections of the transverse and incident shocks, which form a detonation cell, erode the soot and draw more or less regular diamonds [2]. On frontal foils, the head-on impact of the detonation on the foil produces polygonal patterns whose edges represent the positions of the transverse waves at the instant of impact [1, 3–5]. OH PLIF imaging techniques are also becoming a mature tool for investigating the short time- and length-scale phenomena that can participate in the global dynamics of a single cell, e.g. turbulent diffusion and non-relaxed degrees of freedom of radicals, depending on chemical kinetics [6–19]. From a phenomenological point of view, the higher the initial pressure, the larger the number of cells per unit area of the detonation front, given the mixture composition and initial temperature [4, 6, 20, 21].

In channels with constant cross-sectional area, the frontal recordings show irregular patterns if the area or, equivalently, the initial pressure is sufficiently large, regardless of the mixture composition and the cross-sectional shape. However, the parietal recordings may show regular diamonds, depending on the mixture composition [22]. At lower initial pressures or in channels with too small a cross-sectional area, i.e. if there are not enough cells per unit area of the front, the frontal recordings show that the cell patterns depend strongly on the shape of the cross-section. Thus, parietal recordings alone may not fully characterize the cellular structure, and the cell dynamics at the walls of a channel may not represent that of the entire detonation front. Analysis of a sufficiently large number of cells on a parietal recording defines a cell mean width $\bar{\lambda}$. However, a mean width may not be a relevant characteristic length if the cells are too irregular, i.e. if the statistical dispersion of their widths is too large, and may not be physically intrinsic if there are too few cells on the front, i.e. not determined solely by the combustion processes. Whether a mean width is intrinsic and statistically significant depends on the initial pressure, temperature and composition of the mixture, and the transverse dimensions of the channel [1]. When relevant, $\bar{\lambda}$ is a fundamental parameter of detonation dynamics useful in defining criteria of relative detonability. For example, for the self-sustaining propagation, i.e. at velocities close to the theoretical Chapman-Jouguet (CJ) upper limit, there should be at least $\mathcal{O}(100)$ cells on the detonation front surface, i.e. $\mathcal{O}(10)$ on the smaller transverse dimension of the channel. Under these conditions, the determination of cell widths is useful for presizing applied devices such as mitigation systems or detonation-based power generators and propulsive devices, e.g. rotating detonation engines [23–26].

Previous analysis of the cell dynamics during and after the transmission of a detonation from a donor straight channel to a wider receptor channel has classified the transient phenomena of the diffraction processes into three cases, namely supercritical, critical and subcritical. Their common feature is a disturbance propagating inwards from the donor channel locus where the diffraction starts [27]. The diffraction is then supercritical or critical for large enough or not too narrow donor channels, i.e. the cellular structure of the front partially or completely disappears before reinitiation and relaxation to the CJ regime. The subcritical case is that of too narrow donor channels, for which no reinitiation [28] is observed.

Transmission can be abrupt or smooth, depending on whether the transverse dimension of the receptor channel is immediately wider than or increases gradually from the transverse dimension of the donor channel. Most analyses, e.g. [29–33], have dealt with the abrupt transmission. The main result, e.g. [34], is that, in channels with a round cross-section, subcriticality is observed if the donor diameter is less than $\sim \mathcal{O}(10\bar{\lambda})$, depending on the mixture. These limiting values define the critical diameter for detonation transmission, which should not be confused with the much smaller values of those for detonation propagation, i.e. typically $\sim \mathcal{O}(\bar{\lambda})$. For the smooth transmission, i.e. small or moderate expansion angles of the receptor channel, the underlying physics takes place in the reaction zone of the curved part of the diffracted decelerating detonation, which is closer to the wall of the wider channel, in the form of a competition between the rate of loss due to the adiabatic cooling in the transverse expansion and the rate of production due to the adiabatic energy release in the reaction zone. Regardless of whether the expansion angle is large or small, the transverse

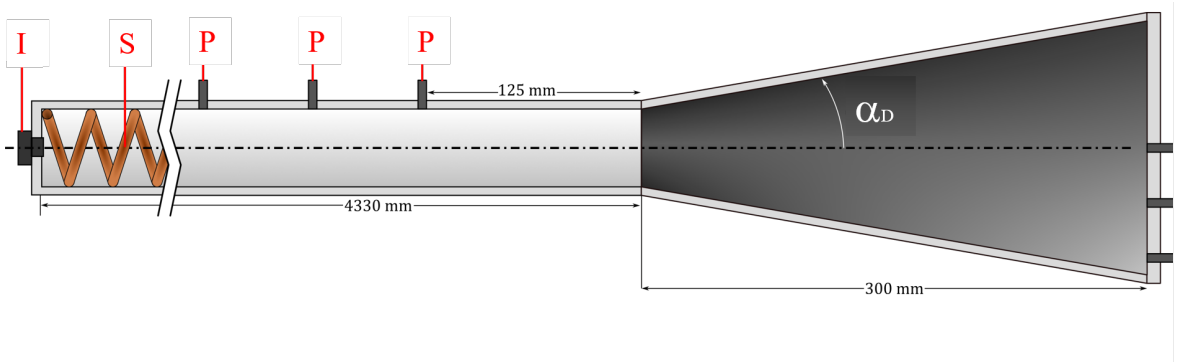

Fig. 1: Schematic of the round or square cross-section setup. I: ignition, S: Shchelkin spiral, P: pressure transducers.

dimension of the donor channel still determines the outcome of the diffraction process, with the mean cell width in the donor channel being the measure of this transverse dimension. In essence, the larger the transverse dimension of the donor channel - the smaller the cell mean width - the easier the transmission, regardless of the expansion angle, i.e. the same expansion angle may or may not result in detonation transmission depending on whether the transverse dimension is large enough or too small.

The analyses for diverging channels with a smoothly increasing round cross-sectional area, e.g. [35–44], have focused on the effects of the initial pressure p_0 and composition of the mixture and the cone half-angle α_D. They show that increasing p_0 or decreasing α_D favors the continuity of the cellular structure. Conversely, decreasing p_0 or increasing α_D favors inward-propagating quenching of the chemical reactions and hence disappearance of the cellular structure. Typically, if $\alpha \geq 60^o$, the detonation behaves as if the area change were abrupt [40].

To our knowledge, there is no data on the effect of the cross-sectional shape for the case of the smooth transmission, which we investigate experimentally in this work, using square and round cross sections. The study extends our previous analysis in straight channels [1, 5] with the stoichiometric mixture $2\,H_2 + O_2 + 2\,Ar$. We had observed that the parietal recordings showed regular diamonds for all initial pressures (p_0) and cross-section shapes considered. However, the frontal recordings showed irregular patterns except for sufficiently low p_0 in the square tube. In that situation, the frontal recordings showed two subsets of transverse waves perpendicular to each other due to their reflection at the channel walls. We consider here this case of low p_0, i.e. with frontal patterns that depend on the cross-sectional shapes, and parietal views that show regular diamonds in constant cross-section channels. We collect data on the three-dimensional transient behaviors of the cellular front during its transmission and propagation in the diverging channels. The observations are based on frontal and parietal cell recordings on soot-coated foils. We interpret the results based on a relation of detonation-shock dynamics between the total curvature and the normal velocity and acceleration of the detonation leading shock [45–47].

Section 2 describes the experimental methodology and the setup. Section 3 describes the recordings, and Section 4 analyses the results and concludes the work.

2 Experimental methodology and setup

We used two experimental setups with the same two-part assembly, i.e. a straight tube and an diverging channel with the same cross-sectional shape, either round or square (Fig. 1). The detonation was initiated at one end of the straight channel, and the diverging channel was positioned at the other. A spark plug or an exploding wire (I) generated a deflagration, and a Shchelkin spiral (S) ensured its transition to detonation at the typical position 1 m relative to the ignition. The straight tubes and the diverging channels were 4.33 m and 300 mm long, respectively, regardless of their cross-sectional shape.

The straight tubes had the same cross-sectional area A_0 =16 cm^2 ± 4%, regardless of their shapes. The entry area of the diverging channels was the same as that of the straight tubes. The rate of area increase $d(A/A_0)/dx$ was the same constant for the round and square diverging channels. This ensures the same area $A(x)$ at the same abscissa x relative to the enlarging section entries, but implies different half-angles, α_D, with constant values 9.8° and 8.7° in the round and square sections, respectively. In our conditions, this choice of small values always ensures the supercritical case of transmission, i.e. continuity of the cellular structure (Sect. 1), which better evidences the high sensitivity of the cell dynamics on the cross-section shape (Sects. 3 and 4).

Parietal and front views of the cellular structure were recorded on soot-coated foils. The parietal foils were positioned along the walls of the straight and diverging channels. The frontal foils were positioned perpendicular to the direction of propagation, at the end of the straight section and at successive abscissas x in the enlarging sections. Thus, one experiment was required for each position x of the frontal foils.

We positioned three piezoelectric pressure sensors (Kistler 603B pressure sensors and 5018A electrostatic charge amplifiers) on the walls of the straight channels before the parietal soot foil and, thus, before the entry of the diverging channels. They were used to obtain an average wave velocity and thus check its steadiness. We also checked steadiness based on the criterion that the cells should have about constant geometric properties before the diverging channels. However, this cannot provide the continuous measurements necessary to obtain a more accurate wave velocity, which would have required, for example, a high-speed camera and transparent channels.

The mixture $2\,H_2 + O_2 + 2\,Ar$ was prepared in a separate tank using the partial-pressure method and then injected at the desired initial pressure p_0 after vacuuming the tubes. The initial pressure p_0 was 20 kPa, and the initial temperature was 294 ± 3 K for all experiments.

3 Description of the results

Figure 2 compares the soot recordings in the round and square diverging channels as a function of the dimensionless cross-sectional area $A(x)/A_0$ (Sect. 2). In the square diverging channel, from $A/A_0 = 1$ to 2, there is no significant effect of the area increase, although the front views show that some of the initially squared patterns are deformed. The initial regularity, i.e. at position $x = 0$, where $A/A_0 = 1$, of the front-view patterns essentially persists, and the cell number remains identical to its value at the channel entry (Sect. 1). The two subsets of transverse waves initially perpendicular to each other, as determined by their reflection at the channel walls, are still present, albeit slightly deformed. From $A/A_0 = 2$, the domains with deformed patterns increases in number, with a stochastic distribution. From $A/A_0 = 4.7$, all patterns on a front view have irregular shapes, i.e. are bounded by transverse waves moving in random directions, i.e. independent of the wall orientation(s). In the round diverging channel, the front views show irregular cells right from the entry of the diverging channel. These trends are qualitatively the same as it would be observed in straight channels with cross sectional area increasing from one experiment to the other at the same initial pressure, or in the same straight channel with initial pressure increasing from one experiment to the other. Qualitatively, the irregularity of the patterns on the front views increases with the cell number, i.e. with increasing cross-sectional area.

Figure 2 shows that the cells are thinner at the beginning of the expansion in the diverging channel with a square cross-section than in the diverging channel with a round cross-section. This difference disappears as the number of cells increases. In a straight channel, given a cross-sectional area with a value lower than the limit above which the shape of the cross-section has no effect, the detonation cells in a square cross-section appear to be thinner than those in a round cross-section [1, 5]. The reason is probably a shorter travel time of perturbations between opposite walls in the square cross-section than between opposite points in the round cross-section. This effect of the cross-sectional shape disappears in large cross-sections because the cell beat time is then much smaller than the perturbation travel time so that the cell dimensions are independent of the cross-sectional shape. In this

work, the cross-sectional area of the straight channel – from which the diverging channel originates – has a smaller value than the limit described above.

However, given the shape of the cross sections, figure 3 clearly shows that the rate of increase in cell number in an diverging channel is lower than the rate deduced from experiments in straight channels, whose cross sectional area increases from one experiment to the next. Put otherwise, given the cross sectional area and shape, the cell number is lower in the diverging channel than in the straight channel. The cell number at the same cross-sectional area depends on both the shape and the expansion angle of the channel.

Figure 4 shows the planar development of two adjacent, i.e. perpendicular, parietal recordings in the square diverging channel (the right parietal recording in Fig. 4 is that in Fig. 2). The red dotted lines emphasizes the successive positions of the two subsets of transverse waves originating from the channel entry. The recordings provide an alternate view of the disappearance of these subsets as the detonation progresses. They also indicate that these subsets have a phase shift, i.e. a variation in the longitudinal positions where their respective front impacts their wall [1].

Figure 5 compares cell widths λ measured in the square (blue symbols) and round (red symbols) diverging channels, and in square and round straight channels (green symbols) with cross-sectional areas 25 and 71 cm^2, respectively. The shape of the symbols represents that of the channel. The cell widths λ are plotted against the dimensionless area $A(x)/A_0$. The higher the color intensity, the larger the number of cells with a given width. The black symbols give the mean cell widths $\bar{\lambda}$ in the diverging channels. The blue and red solid lines are the boundaries of the domains where the cell width deviation from the mean value is lower or equal to the standard deviation.

The cell mean widths $\bar{\lambda}$ are calculated over abscissa intervals $\Delta x = 30$ mm. This value is large enough to include enough cells so that a mean width is significative, and small enough to capture the evolution of this mean width over the channel length. Thus, the characteristic displacement time of the wave front between the positions x where A/A_0 and the cell number are measured is larger than the characteristic beat time of the cells, and the axial or transverse variations of the cell number with increasing x or A/A_0 result in non ambiguous changes of the cell width. The non-dimensional areas used for positioning $\bar{\lambda}$ on the plot are mean values $\bar{A}(x)$ over the abscissa intervals Δx defined by

$$\bar{A}(x) = \frac{1}{\Delta x} \int_x^{x+\Delta x} A(x)dx, \qquad (1)$$

and the notation A from now designates $\bar{A}$.

Regardless of the cross-sectional shape, $\bar{\lambda}$ increases with increasing A/A_0, before decreasing from $A/A_0 \sim 3$ to stabilize at the same value $\bar{\lambda} \sim 11 \pm 0.5$ mm, which is higher than the value of ~ 9 mm obtained for the largest straight tube (71 cm^2) where the influence of the section shape would be negligible [1].

The values of $\bar{\lambda}$ are larger, and the position of their maximum is lower, in the round diverging channel. The largest values of $\bar{\lambda}$ are ~ 15 and ~ 12.5 mm, and their positions correspond to the dimensionless areas A/A_0 of 2.5 and 3, in the round and square channels, respectively. The mean cell width becomes independent of the cross-section shape from the abscissa x where $A/A_0 \sim 6$, consistent with the observation from Figure 2 that irregular patterns then cover the entire front surface. These trends are essentially the same as for a straight tube, i.e. the larger the area, the lower the effect of the shape on $\bar{\lambda}$.

Figure 6 shows the number of cells as a function of the dimensionless area A/A_0. This number is approximately constant from the entry of the diverging channels to the abscissa x, where $A/A_0 \sim 3$, consistent with their increasing values (Fig. 5). Although the increase is monotonic, the comparison of Figures 6 and 5 shows no obvious relationship between the number and width of the cells. In fact, the cell number for the smaller areas A/A_0 – or abscissa x – is smaller for the round section than for the square section, but larger for the larger A/A_0. In contrast, Figure 5 shows that the cell width is always larger in the round section, regardless of A/A_0, and only asymptotically the same for the larger A/A_0.

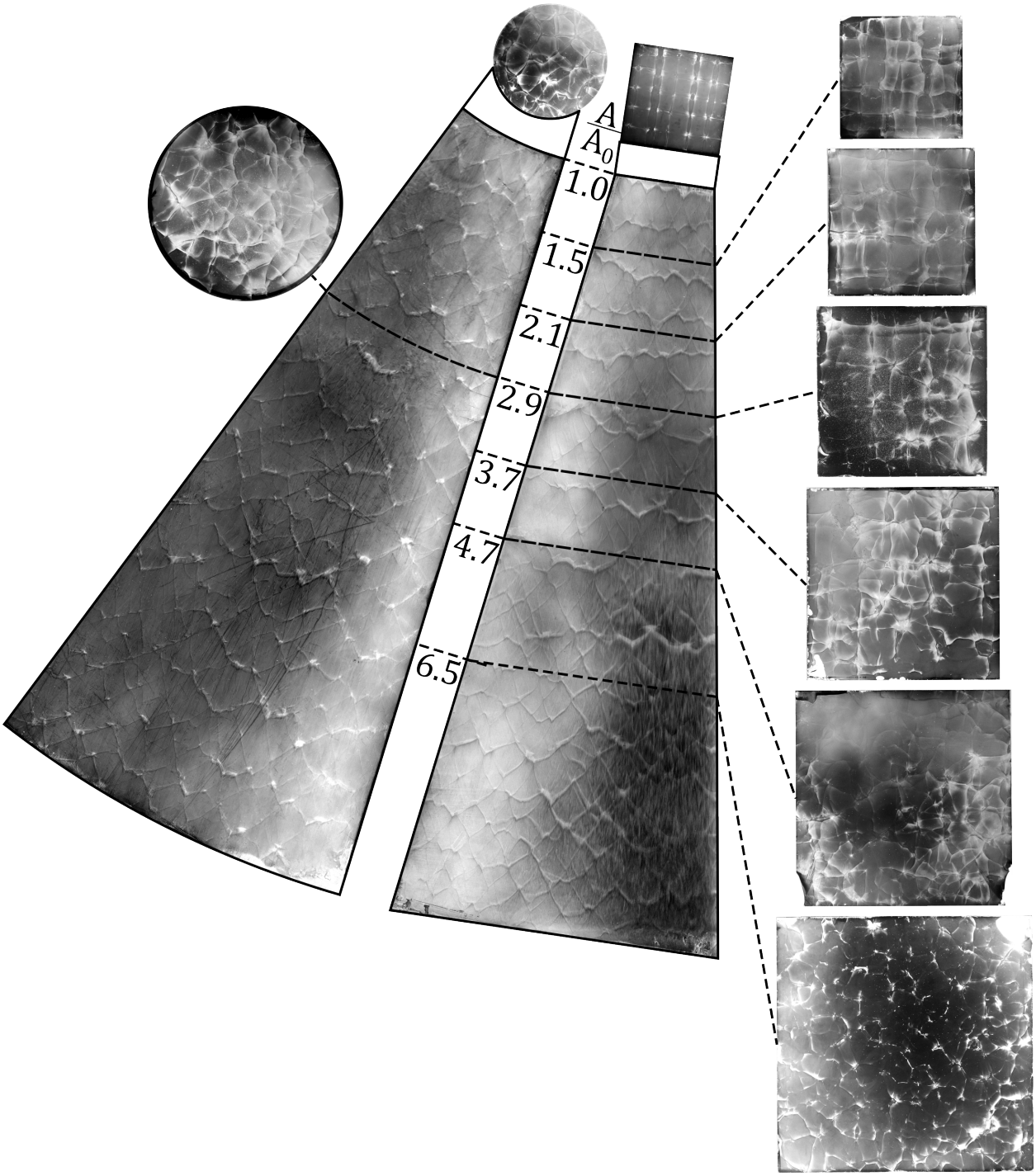

Fig. 2: Parietal and frontal recordings of detonation cellular structures in the round tube (left) and in the square tube (right). The cross-sectional areas have the same initial value $A_0 = 16$ cm^2 and the same rate of increase. Mixture: $2\,H_2 + O_2 + 2\,Ar$. Initial pressure: p_0=20 kPa. Initial temperature: T_0=294 K.

4 Discussion and conclusion

Gubin and Kogarko [37] had conducted a series of experiments in a round cross-sectional diverging channel attached to a 32 mm diameter straight

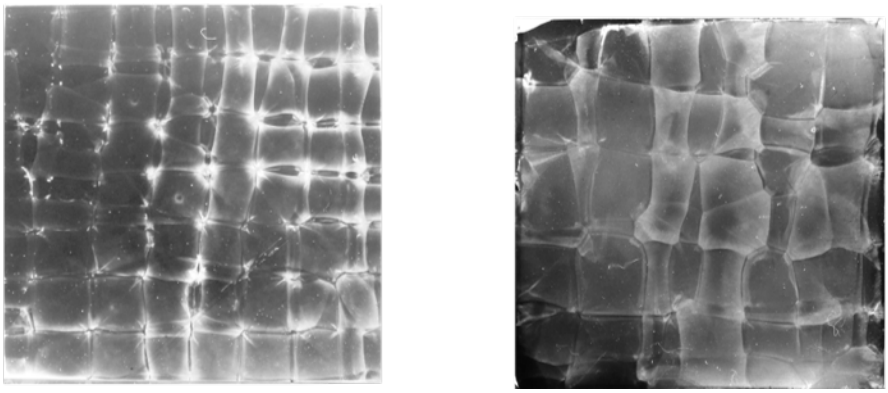

Fig. 3: Frontal recordings of detonation cellular structures at cross-sectional area of 50×50 mm^2. Left: straight channel, i.e. constant area. Right: diverging channel, i.e. increasing area, here at the position $A/A_0 = 1.5$ in Figure 2. Mixture: $2\,H_2 + O_2 + 2\,Ar$. Initial pressure: p_0=20 kPa. Initial temperature: T_0=294 K.

tube, and with an expansion half-angle of 60° or 45°. They reported supercritical transmissions (Section 1) with non-monotonic evolution of the front perturbations (presumably $\sim \lambda$) similar to those shown in Figure 5, with the detonation velocity D first decreasing and then increasing. They indicated these effects were all the smaller the higher the initial pressure was.

The present results show that, at constant initial pressure, using different cross-sectional shapes produces similar effects on $\bar{\lambda}$. They also bring out the long relaxation time of $\bar{\lambda}$ after the shape effect has vanished. The analysis below offers a plausible interpretation based on the relation of Detonation Shock Dynamics (DSD) [45–47].

$$\frac{\delta D}{\delta t} = V^2\,(W - \kappa)\,, \tag{2}$$

which includes the effects of the normal velocity D, normal acceleration $\delta D/\delta t$ and total curvature κ of the front. Relation (2) is valid only for self-sustained detonations, i.e. with a sonic locus far enough away from the average leading shock of the detonation so that the extent of chemical evolution is large enough. This means that it can describe only global dynamics of wave fronts subjected to small changes of the boundary conditions during the propagation of the detonation. That is the case here since the half-angles of the diverging channels are small (Sect. 2). The terms V^2 and W are strictly positive with dimensions of a square velocity and a reciprocal of a length, respectively. Relation (2) has a hyperbolic structure (a telegrapher-like second-order differential equation for the front surface), so V represents the velocity of a perturbation propagating on the front surface, and V/D is the tangent of the local half-angle α_M of its Mach cone. The term W relates to chemical kinetics. Relation (2) embeds the classical $D - \kappa$ relation, e.g. [48–50], which is valid only for very weakly curved waves, i.e. with a very large radius of curvature compared to the characteristic chemical length (the distance from the shock to the sonic locus), so that the acceleration effect is negligible.

There are several versions of this relation, but with different expressions for V and W, which, however, have the same qualitative behaviors. The simplest are obtained in the limit of high activation energies of the chemical process and in the approximation of a constant ratio γ of the specific heats [47],

$$V(D) = \sqrt{\frac{2\gamma^2}{4\gamma^2 + \gamma - 3}} \times D \tag{3}$$

$$W(D) = \frac{\gamma^2 - 1}{8\gamma^2}\left(\left(\frac{D_{CJ}}{D}\right)^2 - 1\right) \times \frac{1}{\ell(D)}, \tag{4}$$

where $\ell(D)$ is the induction length behind a planar shock with constant velocity D, a decreasing function with increasing D. The large activation energy assumption provides qualitatively correct wave dynamics but cannot produce quantitative reliable information. Therefore, our DSD analysis

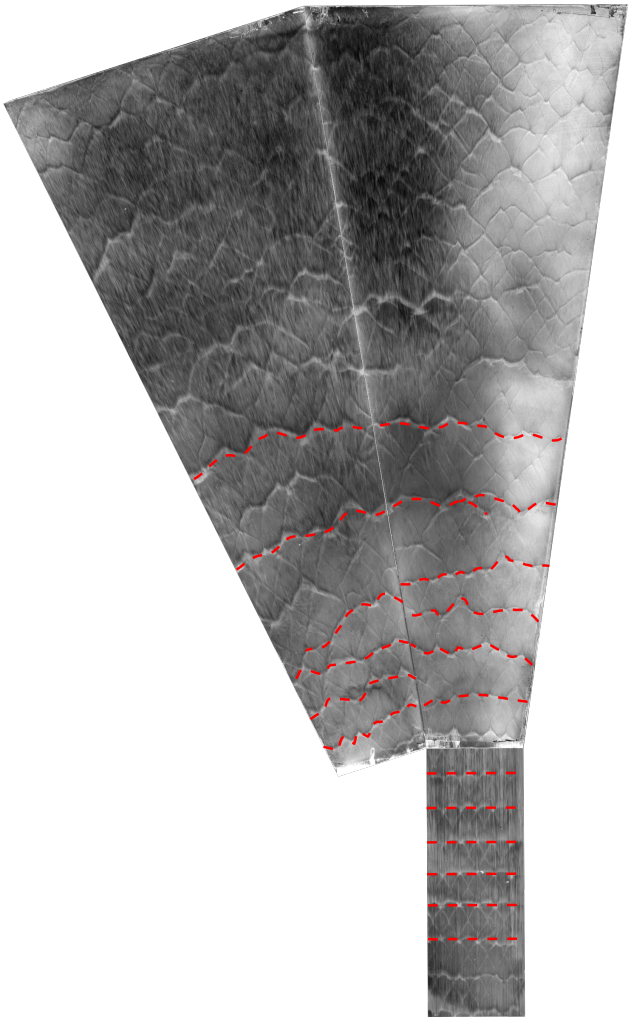

Fig. 4: Parietal recordings at two adjacent walls in the square diverging channel. The red dashed lines show the increasing irregularity of the transverse wave impacts with increasing area.

is not quantitative and focuses on the qualitative interpretation of the soot recordings.

Typical values of γ ranging between 1.1 and 1.3 give local Mach angles α_{M} that are not more than a few degrees different from $\sim 40^{\mathrm{o}}$. This value is much larger than the channel expansion angles $\alpha_{\mathrm{D}} \sim 10^{\mathrm{o}}$ Section 2, which, mathematically, ensures that the analysis of the wave front dynamics based on Relation (2) is a well-posed problem, i.e., physically, that the perturbations from the walls act on the wave front dynamics (Fig. 7).

The identity $\delta D/\delta t = R^{-1}\delta D/\delta R$, with $\kappa = j/R$, and $j = 0, 1$ or 2 for planar, cylindrical or spherical wave fronts, gives the 1^{st}-order differential equation

$$\frac{\delta D}{\delta R}(D,R) = \frac{V^2(D)}{D}\left(W(D) - j/R\right), \qquad (5)$$

whose integral curves are relations between the wave velocity D and its position R (or its total curvature κ), and the initial conditions a constraint between given values of D and R.

Figure 8 shows a scheme with an integral curve starting from the $D-R$ initial condition represented by point S. The arrows indicate the increasing times, since the wave expands ($dR > 0, d\kappa < 0$). The dashed curve is the $D - \kappa$ relation without

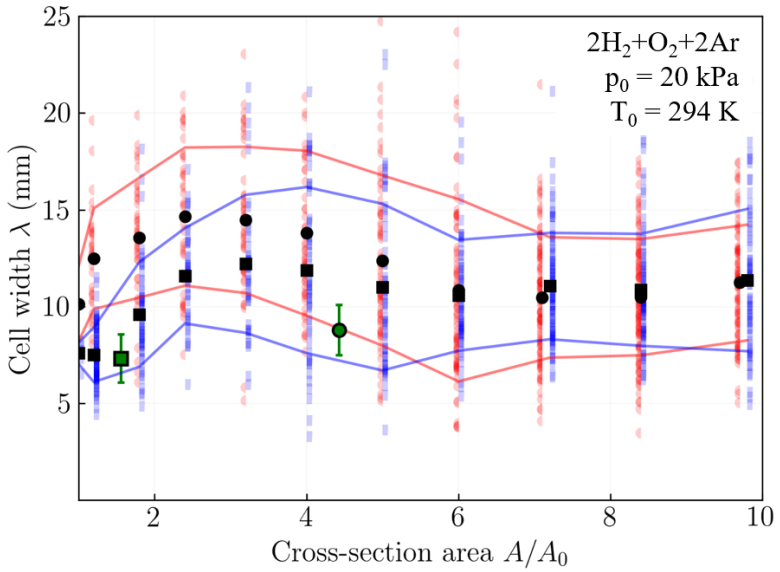

Fig. 5: Cell widths λ measured in the increasing area sections as a function of the dimensionless area $A(x)/A_0$. The shape of the symbols is that of the cross-section. Blue: square diverging channel with A_0 =16 cm^2. Red: round diverging channel with A_0 =16 cm^2. Green: constant cross-section tubes. Full-line curves with the same color delimit measurements with dispersion lower than the standard deviation.

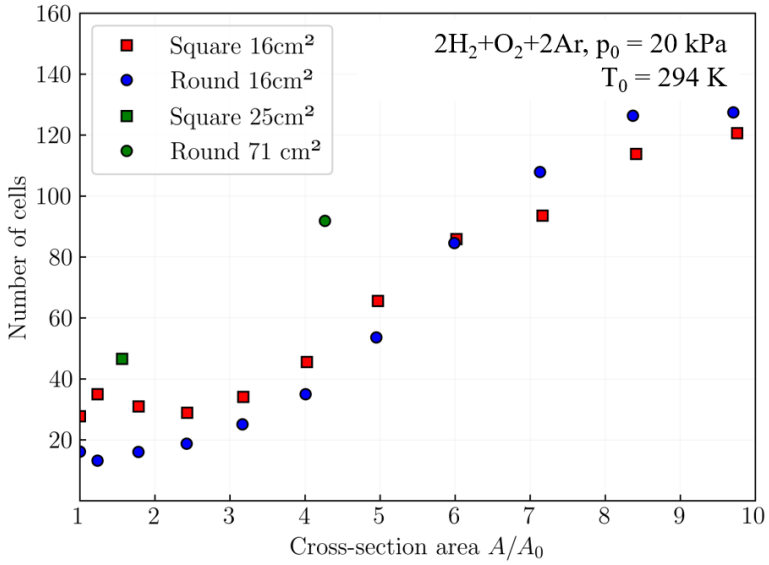

Fig. 6: Cell number as a function of the dimensionless area $A(x)/A_0$.

the acceleration effect, which separates waves that decelerate (on its right) from those that accelerate (on its left).

Before diffraction, because of our choice that the cellular detonations in the straight channels have a cell dynamics depending on the cross-sectional shapes, the average shape of the detonation front

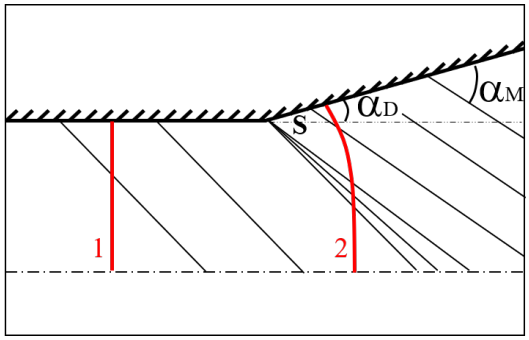

Fig. 7: Scheme of the diffraction process. Red lines: average detonation front before (1) and during (2) the diffraction. Thin black lines: characteristic (Mach) lines (shown as straight lines for simplification).

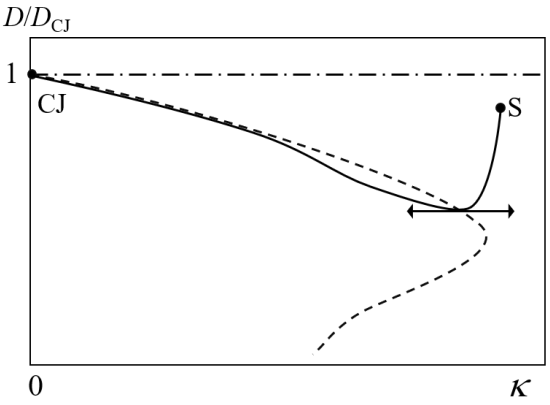

Fig. 8: Diffracting detonation dynamics in the Velocity D - Curvature κ plane. Full line: integral curve from the initial condition at point S. Dashed line: 0-acceleration curve.

close to the wall should be considered as only quasi-planar ($\kappa \gtrsim 0$) and therefore its normal velocity close to the CJ value ($D \lesssim D_{\rm CJ}$). Immediately after diffraction, the sudden transverse expansion of the flow, necessary for its adaptation to the diverging wall(s) forces this curved part of the front to decelerate, hence the initial condition represented by point S. Thus, the initial effect of curvature is necessarily greater than that of energy production, i.e $\kappa > W$, so $\delta D/\delta t \propto \delta D/\delta R < 0$ from (2) or (5). As the wave expands, although the velocity decreases, the curvature of the wave also decreases, and its effect eventually becomes less than that of the chemical production term W after the integral curve has reached the 0-acceleration $D - \kappa$ curve. The front then accelerates up to the CJ point, i.e. $\kappa < W$, so $\delta D/\delta t \propto \delta D/\delta R > 0$. Since the mean cell width λ is all the greater the smaller the velocity of the average detonation front, this explains the non-monotonic behaviors in Figure 5.

Relations (2) or (5) also suggest a plausible explanation for why the cell mean widths are larger in the round cross-section at the beginning of the diffraction process and why this difference vanishes as the wave progresses. In fact, simple geometry indicates that the curvatures of the diffracted fronts are necessarily greater in a round cross-section than in a square cross-section. For example, the total curvature of a spherical wave is twice that of a cylinder of the same radius. Therefore, here, the deceleration is greater in the round tube, resulting in locally lower velocities and hence larger chemical lengths and cells. Equivalently, the rate of increase in cell width is greater in the round diverging channel. As the cell widths are initially larger in the round channel under our conditions, the mean width values will increase faster and have larger values than in the square section. As the wave progresses, the deceleration effect disappears, and the only remaining effect is that of the vanishing small expansion. That explains both why the cell widths tend to be asymptotically the same at large values of A/A_0 and why this asymptotic value is larger than in the straight entry channels. Indeed, Figure 5 shows that for the cross section $A/A_0 \sim 4.5$ ($A = 71$ cm^2), the cell widths in the square and round diverging channels, i.e. ~ 11 and ~ 13 mm, are larger than the width ~ 9 mm measured in the constant cross-section channel with the same cross-sectional area A (round green symbol). The effect of the wave front curvature seems to have a very long characteristic time of disappearance, so that much longer channels are certainly necessary to reach the intrinsic cell width corresponding to the CJ detonation, i.e. the planar wave.

Based on the cell width variation in the enlarging section, the velocity variations are certainly very small. This can be observed from the approximation $\lambda \propto E/RT$ where λ is the cell width, E is the activation energy, R is the gas constant, and T is the shock temperature. With $T \propto D^2$ (D the average front velocity), this gives $\Delta\lambda/\lambda = 2(E/RT)\Delta D/D$, that is, $\Delta D/D \sim (\Delta\lambda/\lambda)/20$ using a typical value $E/RT = \mathcal{O}(10)$. In our experiments, we measured

variations $\Delta\lambda/\lambda \sim \mathcal{O}(0.1)$, suggesting values of $\Delta D/D$ less than 1%.

Experiments in a narrow diverging channel with a nonlinearly enlarging rectangular cross-section and a high expansion rate are described in [51, 52] and analyzed with a $D(\kappa)$ DSD modeling, i.e., without acceleration effect. Our experiments show non-monotonic variations of the cell width at the wave entries in the enlarging channels (Figs. 5 and 6), which requires a modeling that includes this effect. In addition, our diverging channels have square or round cross-sectional shapes, i.e., without a narrowest dimension that would constrain the cell dynamics. Finally, we emphasize that our expansion rate is low (Sect.2).

In conclusion, this experimental work and its detonation-shock-dynamics interpretation show that the transient dynamics of three-dimensional detonation cells is very sensitive to small changes in the boundary conditions and that, in particular, it takes a long time for the cellular dynamics to become independent of the geometry of diverging channels. This sensitivity also makes the data collected in this work a relevant experimental basis for high-resolution numerical simulations capable of handling three-dimensionality and detailed chemical kinetics mechanisms. It emphasizes that the conditions for measuring detonation cell widths require constant cross-section tubes of sufficient size and length. Inductively, representing three-dimensional cells requires more statistical descriptors than a single mean width.

Acknowledgements

This work was supported by the Ministry of Higher Education, Research and Innovation (France)

References

[1] V. Monnier, V. Rodriguez, P. Vidal, R. Zitoun, An analysis of three-dimensional patterns of experimental detonation cells, Combustion and Flame 245 (2022) 112310. doi:10.1016/j.combustflame.2022.112310.

[2] P. V. Tiggelen, J. Libouton, Évolution des variables chimiques et physiques à l'intérieur d'une maille de détonation, Annales de Physique Fr. 14 (1989) 649 – 660. doi:10.1051/anphys:01989001406064900.

[3] Y. N. Denisov, Y. K. Troshin, Pulsating and spinning detonation of gaseous mixtures in tubes, Dokl. Akad. Nauk SSSR 125 (1959) 110–113.

[4] B. Voitsekhovskii, V. Mitrofanov, M. Topchian, Trad: The structure of the detonation front in gases, SO AN SSSR (1963).

[5] V. Monnier, V. Rodriguez, P. Vidal, R. Zitoun, Experimental analysis of cellular detonations: regularity and 3d patterns depending on the geometry of the confinement, Proc. 28$^{\text{th}}$ ICDERS, Paper 57 (2022).

[6] R. Strehlow, R. Liaugminas, R. Watson, J. Eyman, Transverse wave structure in detonations, Symposium (International) on Combustion 11 (1) (1967) 683–692. doi:10.1016/S0082-0784(67)80194-2.

[7] R. A. Strehlow, R. E. Maurer, R. S., Transverse waves in detonations: I. Spacing in the Hydrogen-Oxygen System, AIAA J. 7 (1969) 323–328. doi:10.2514/3.5093.

[8] R. A. Strehlow, C. D. Engel, Transverse waves in detonations: II. Structure and spacing in H_2-O_2, $C_2H_2-O_2$, $C_2H_4-O_2$ and CH_4-O_2 systems, AIAA J. 7 (1969) 492–496. doi:10.2514/3.5134.

[9] R. Soloukhin, Nonstationary phenomena in gaseous detonation, Symp. (Int.) Combust. 12 (1) (1969) 799–807. doi:10.1016/S0082-0784(69)80461-3.

[10] V. A. Subbotin, Two kinds of transverse wave structures in multifront detonation, Combustion, Explosion and Shock Waves 11 (1975) 83–88. doi:10.1007/BF00742862.

[11] F. Pintgen, Laser-optical visualization of detonation structures, Ph.D. thesis, Diplom Arbeit, Lehrstuhl für Thermodynamik: Technische Universität München/Graduate Aeronautical Laboratories: California Institute of Technology (2000).

[12] S. Singh, D. Lieberman, J. E. Shepherd, Combustion behind shock waves, Combustion Institute (2003), Paper 03F-29 Western States Section.

[13] M. Short, G. J. Sharpe, Pulsating instability of detonations with a two-step chain-branching reaction model: theory and numerics, Combust. Theor. Model. 7 (2) (2003) 401–416. doi:

10.1088/1364-7830/7/2/311.

[14] J. Austin, F. Pintgen, J. Shepherd, Reaction zones in highly unstable detonations, Proceedings of the Combustion Institute 30 (2) (2005) 1849–1857. doi:10.1016/j.proci.2004.08.157.

[15] M. I. Radulescu, G. J. Sharpe, C. K. Law, J. H. S. Lee, The hydrodynamic structure of unstable cellular detonations, Journal of Fluid Mechanics 580 (2007) 31–81. doi:10.1017/S0022112007005046.

[16] B. M. Maxwell, R. R. Bhattacharjee, S. S. M. Lau-Chapdelaine, S. A. E. G. Falle, G. J. Sharpe, M. I. Radulescu, Influence of turbulent fluctuations on detonation propagation, Journal of Fluid Mechanics 818 (2017) 646–696. doi:10.1017/jfm.2017.145.

[17] K. Chatelain, R. Mével, J. Melguizo-Gavilanes, A. Chinnayya, S. Xu, D. A. Lacoste, Effect of incident laser sheet orientation on the oh-plif imaging of detonations, Shock Waves 30 (2020) 688–702. doi:10.1007/s00193-020-00963-y.

[18] S. B. Rojas Chavez, K. P. Chatelain, T. F. Guiberti, R. Mével, D. A. Lacoste, Effect of the excitation line on hydroxyl radical imaging by laser induced fluorescence in hydrogen detonations, Combustion and Flame 229 (2021) 111399. doi:10.1016/.combustflame.2021.111399.

[19] S. B. R. Chavez, K. P. Chatelain, M. Alicherif, D. A. Lacoste, Characterization of detonation waves by simultaneous oh and no planar laser-induced fluorescence, Applications in Energy and Combustion Science 18 (2024) 100257. doi:10.1016/j.jaecs.2024.100257.

[20] P. J. Van Tiggelen, J. C. Libouton, Evolution des variables chimiques et physiques à l'intérieur d'une maille de détonation, Ann. Phys. 14 (1989) 649–660.

[21] G. J. Sharpe, J. J. Quirk, Nonlinear cellular dynamics of the idealized detonation model: Regular cells, Combust. Theor. Model. 12 (2008) 1–21. doi:10.1080/13647830701335749.

[22] V. I. Manzhalei, V. V. Mitrofanov, V. A. Subbotin, Measurement of inhomogeneities of a detonation front in gas mixtures at elevated pressures, Combustion, Explosion and Shock Waves 10 (1974) 89–95. doi:10.1007/BF01463793.

[23] F. A. Bykhovskii, Continuous spin detonations, J. Propuls. Power 22 (2006) 1204–1216. doi:10.2514/1.17656.

[24] P. Wolanski, Detonative propulsion, Proceedings of the Combustion Institute 34 (1) (2013) 125–158. doi:10.1016/j.proci.2012.10.005.

[25] S. Hansmetzger, R. Zitoun, P. Vidal, Detonation regimes in a small-scale rde, in: Proceedings of the 26th International Colloquium on the Dynamics of Explosions and Reactive Systems, 1037, 2017.

[26] P. Hellard, T. Gaillard, D. Davidenko, Transitory injection simulation to study injector performance of an experimental rotating detonation engine, in: IWDP 2022, Berlin, Germany, 2022.

[27] D. Desbordes, C. Guerraud, L. Hamada, H. Presles, Failure of the classical dynamic parameters relationships in highly regular cellular detonation systems, AIAA Prog. Astronaut. Aeronaut. 153 (1993) 347–359.

[28] V. Guilly, Etude de la diffraction de la détonation des mélanges C_2H_2 / O_2 stoechiometriques dilués par l'argon, Ph.D. thesis, Université de Poitiers (2007).

[29] D. H. Edwards, G. O. Thomas, M. A. Nettleton, The diffraction of a planar detonation wave at an abrupt area change, J. Fluid Mech. 95 (1979) 79–96. doi:10.1017/S002211207900135X.

[30] Y. Liu, J. Lee, R. Knystautas, Effect of geometry on the transmission of detonation through an orifice, Combustion and Flame 56 (2) (1984) 215–225. doi:10.1016/0010-2180(84)90038-5.

[31] E. Pantow, M. Fischer, T. Kratzel, Decoupling and recoupling of detonation waves associated with sudden expansion, Shock Waves 6 (1996) 131–137. doi:10.1007/BF02510993.

[32] A. Fedorov, T. Khmel, Y. Kratova, Shock and detonation wave diffraction at a sudden expansion in gas–particle mixtures, Shock Waves 18 (2007) 281–290. doi:10.1007/s00193-008-0162-x.

[33] V. Levin, I. Manuylovich, V. Markov, Cellular structure of divergent cylindrical detonation waves, Dokl. Phys. 56 (2011) 391–393. doi:10.1134/S1028335811070020.

[34] R. Knystautas, J. Lee, C. Guirao, The critical tube diameter for detonation failure in hydrocarbon-air mixtures, Combustion and Flame 48 (1982) 63–83. doi:10.1016/0010-2180(82)90116-X.

[35] S. M. Kogarko, On the possibility of detonation of gaseous mixtures in conical tubes, Izv. Akad. Nauk SSSR, Otd. Khim. Nauk 4 (1956) 419–426.

[36] S. A. Gubin, S. M. Kogarko, V. N. Mikhalkin, Experimental study of gas detonation in conical tubes, Translated from Fizika i Vzryva 18 (1981) 111–117. doi:10.1007/BF00800631.

[37] S. A. Gubin, S. M. Kogarko, V. N. Mikhalkin, Experimental study of gas detonation in conical tubes, Combustion, Explosion and Shock Waves 18 (1982) 592–597. doi:10.1007/BF00800631.

[38] R. A. Strehlow, R. J. Salm, The failure of marginal detonations in expanding channels, Acta Astronautica 3 (11) (1976) 983–994. doi:10.1016/0094-5765(76)90007-2.

[39] G. Thomas, D. H. Edwards, J. H. Lee, R. Knystautas, I. O. Moen, Y. M. Wei, Detonation diffraction by divergent channels, in: Dynamics of Explosions, J.-C. Leyer and R.I. Soloukhin and J.R. Bowen, 1986, pp. 144–154. doi:10.2514/5.9781600865800.0144.0154.

[40] A. Borisov, S. V. Khomik, E. V. Saneevt, Critical energy of direct detonation initiation in gaseous mixtures, in: Dynamics of Detonations and Explosions: Detonations, Vol. 133, AIAA, 1989, pp. 142–155. doi:10.2514/5.9781600866067.0142.0155.

[41] V. Guilly, B. Khasainov, H. N. Presles, D. Desbordes, Influence de la dilution par l'argon d'un mélange C_2H_2 / O_2 sur les conditions critiques de diffraction de sa détonation, Mécanique et industrie 196 (2005) 269–273. doi:10.1051/meca:2005028.

[42] B. Khasainov, H.-N. Presles, D. Desbordes, P. Demontis, P. Vidal, Detonation diffraction from circular tubes to cones, Shock Waves 14 (2005) 187–192. doi:10.1007/s00193-005-0262-9.

[43] R. Sorin, R. Zitoun, B. Khasainov, D. Desbordes, Detonation diffraction through different geometries, Shock Waves 19 (2009) 11–23. doi:10.1007/s00193-008-0178-1.

[44] T. Endo, R. Kobayashi, S. Kuwajima, Y. Seki, W. Kim, T. Johzaki, Detonation propagation from a cylindrical tube into a diverging cone, Journal of Thermal Science and Technology 15 (2020). doi:10.1299/jtst.2020jtst0030.

[45] L. Brun, Une théorie de la détonation dans les explosifs condensés fondée sur l'hypothèse de Jouguet (1989), Rapport CEA/DAM DPM/BS 224/89.

[46] A. Kasimov, D. Stewart, Asymptotic theory of evolution and failure of self-sustained detonations, J. Fluid Mech. 525 (2005) 161–192. doi:10.1017/S0022112004002599.

[47] P. Vidal, Critical slow dynamics of detonation in a gas with non-uniform initial temperature and composition: a large activation-energy analysis, International Journal of Spray and Combustion Dynamics (IJSCD) 1(2) (2009) 435–471. doi:10.1260/175682709789685822.

[48] W. W. Wood, J. G. Kirkwood, Diameter effect in condensed explosives. the relation between velocity and radius of curvature of the detonation wave, J. Chem. Phys. 2(11) (1954) 1920–1924. doi:10.1063/1.1739940.

[49] J. B. Bdzil, D. S. Stewart, Theory of detonation shock dynamics, In: Zhang, F. (eds) Shock Waves Science and Technology Library, Vol. 6. Shock Wave Science and Technology Reference Library, vol 6. Springer, Berlin, Heidelberg. (2012)doi:10.1007/978-3-642-22967-1_7.

[50] M. Short, S. J. Voelkel, C. Chiquete, Steady detonation propagation in thin channels with strong confinement, J. Fluid Mech. 889, *A3* (2020). doi:10.1017/jfm.2020.37.

[51] M. I. Radulescu, B. Borzou, Dynamics of detonations with a constant mean flow divergence, Journal of Fluid Mechanics 845 (2018) 346–377. doi:10.1017/jfm.2018.244.

[52] Q. Xiao, M. I. Radulescu, Dynamics of hydrogen–oxygen–argon cellular detonations with a constant mean lateral strain rate, Combustion and Flame 215 (2020) 437–457. doi:https://doi.org/10.1016/j.combustflame.2020.01.041.